Journal of
Composites Science

MDPI

Article

Innovative Carbon-Doped Composite Pavements with Sensing Capability and Low Environmental Impact for Multifunctional Infrastructures

Hasan Borke Birgin [1], Antonella D'Alessandro [1,*], Simon Laflamme [2] and Filippo Ubertini [1]

[1] Department of Civil and Environmental Engineering, University of Perugia, Via Goffredo Duranti 93, 06125 Perugia, Italy; hasanborke.birgin@unipg.it (H.B.B.); filippo.ubertini@unipg.it (F.U.)
[2] Department of Civil, Construction and Environmental Engineering, Iowa State University, Ames, IA 50011, USA; laflamme@iastate.edu
* Correspondence: antonella.dalessandro@unipg.it; Tel.: +39-0755853910

Abstract: Recently, smart composites that serve as multi-functional materials have gained popularity for structural and infrastructural applications yielding condition assessment capabilities. An emerging application is the monitoring and prediction of the fatigue of road infrastructure, where these systems may benefit from the ability to detect and estimate vehicle loads via weigh-in-motion (WIM) sensing without interrupting the traffic flow. However, off-the-shelf applications of WIM can be improved in terms of cost and durability, both on the hardware and software sides. This study proposes a novel multi-functional pavement material that can be utilized as a pavement embedded weigh-in-motion system. The material consists of a composite fabricated using an eco-friendly synthetic binder material called EVIzero, doped with carbon microfiber inclusions. The composite material is piezoresistive and, therefore, has strain-sensing capabilities. Compared to other existing strain-sensing structural materials, it is not affected by polarization and exhibits a more rapid response time. The study evaluates the monitoring capabilities of the novel composite according to the needs of a WIM system. A tailored data acquisition setup with distributed line electrodes is developed for the detection of moving loads. The aim of the paper is to demonstrate the sensing capabilities of the newly proposed composite pavement material and the suitability of the proposed monitoring system for traffic detection and WIM. Results demonstrate that the material is promising in terms of sensing and ready to be implemented in the field for further validation in the real world.

Keywords: weigh-in-motion; smart materials; multifunctional composites; pavement composites; load sensing; piezo-resistive materials; structural health monitoring; carbon fillers; conductive pavements; traffic load monitoring; road infrastructure monitoring; fatigue life

check for updates

Citation: Birgin, H.B.; D'Alessandro, A.; Laflamme, S.; Ubertini, F. Innovative Carbon-Doped Composite Pavements with Sensing Capability and Low Environmental Impact for Multifunctional Infrastructure. *J. Compos. Sci.* **2021**, *5*, 192. https://doi.org/10.3390/jcs5070192

Academic Editors: Marco Monti, Ilaria Armentano and Francesco Tornabene

Received: 25 May 2021
Accepted: 16 July 2021
Published: 20 July 2021

Publisher's Note: MDPI stays neutral with regard to jurisdictional claims in published maps and institutional affiliations.

Copyright: © 2021 by the authors. Licensee MDPI, Basel, Switzerland. This article is an open access article distributed under the terms and conditions of the Creative Commons Attribution (CC BY) license (https://creativecommons.org/licenses/by/4.0/).

1. Introduction

Measuring traffic loads on road infrastructures can be useful for improving the accuracy of fatigue estimation of critical structures, in particular bridges [1–5], that are prone to traffic-induced fatigue accumulation that could lead to sudden failure [6]. Weigh-in-motion (WIM) sensors [7–9] can be used to measure the type and magnitude of traffic loads, providing key data on daily usage and on effects of extraordinary events and improving condition-based maintenance decisions [10]. Popular WIM sensors reported in the literature include bending plates [11], load cells [12], piezoelectric sensors [13,14] and in-pavement fiber Bragg gratings (FBGs) [15]. The specialization to bridge applications, also known as bridge WIM or B-WIM, is often conducted by measuring the bridge's deformations using strain sensors [16–20], accelerometers [21–23], or computer vision systems [24].

Widespread applications of WIM sensors and systems require non-intrusive, low-cost, and durable solutions capable of accurately detecting vehicle types and estimating their speed and weight through the axle count, weight, and separations [9,14,25,26]. The use of

multi-functional materials capable of sensing as non-intrusive and highly durable solutions has been studied by the authors and other researchers [27–32]. Challenges in using these smart materials reside in formulating scalable solutions for WIM characterized by low cost and ease of fabrication and installation.

Multi-functional composites, also known as smart materials, are often engineered using cementious matrices [33–36]. The polarization of the matrices is a critical issue that requires special attention in WIM sensing applications [37]. Other non-cementitious matrices have been proposed in the literature, including, unsaturated polyester resin [38], epoxy [39], green alkali-activated binders [40] and asphalt concrete with carbon inclusions capable of strain sensing [41–43].

Here, the study evaluates the use of an industrial sustainable pavement binder composite, termed EVIzero [44], in fabricating smart pavements capable of WIM sensing. The EVIzero based composite proposed by the authors has not been investigated in the available literature and represents a novelty in the scientific panorama. The EVIzero is doped with carbon microfibers which confer the pavement with piezo-resistive properties producing measurable electrical responses provoked by traffic-induced deformations. This composite has the combined advantages of high durability and scalability, and does not suffer from the polarization effect found in typical cementitious materials. The sensor is also equipped with distributed electrodes that are designed for detecting the moving loads. This type of configuration was never explored before and is foreseen to be effective in terms of reducing the number of sensing units within WIM systems. The study focuses on the load sensing capability of such a monitoring layout.

The objective of the research is to evaluate: (1) the sensing capability of the novel composite; (2) the performance of the smart pavement at WIM sensing through the detection and quantification of the axles of the vehicles; and (3) the optimal configuration for WIM applications. The investigation is conducted on medium scaled sections of 30 cm × 20 cm × 3.5 cm subjected to various loads including (1) hammer impact loads located on different parts of the sample surface; (2) rapid loading–unloading tests with varying loads; and (3) traffic loads produced from light vehicles at various speeds.

The rest of the paper is organised as follows. Section 2 explains the production of material and laboratory test methodology. Section 3 discusses the electric features of material and introduces the electromechanical test results together with the results from WIM characterization tests. Section 4 discusses the obtained results and functionality of the composite. Section 5 concludes the paper.

2. Materials and Methods

2.1. Pavement Fabrication

Materials used in the fabrication of the smart pavement consist of a binder material (EVIzero) developed by Corecom s.r.l. [44], aggregates from Ancona-Bianco (Italy), and CMF SIGRAFIL from SGL Carbon [45]—they are cut carbon fibers with a diameter of 7 µm and length of 6 mm. Electrodes used in connecting to the data acquisition system (DAQ) consist of 1 mm diameter copper wires. EVIzero is a granular, neutral colored synthetic binder based on polyolefin and fabricated using polymers and industrial by-products. The key material characteristics are listed in Table 1.

Table 1. Material characteristics for EVIzero [44], CMF [45] and copper.

Feature	EVIzero	CMF	Copper
conductivity ($S \cdot m^{-1}$)	-	6.67×10^4	58.7×10^6
density (g/cm^3)	0.85	1.80	8.96
melting point (°C)	75	3600	1085
mixing temperature (°C)	160–170	-	-
dynamic viscosity at 160 °C (mPa·s)	700	-	-

Figure 1 illustrates the fabrication process. First, aggregates are sieved and separated into fine (between 0.5 and 2 mm) and coarse (between 2 and 8 mm) ones. Materials are weighted according to quantities listed in Table 2.

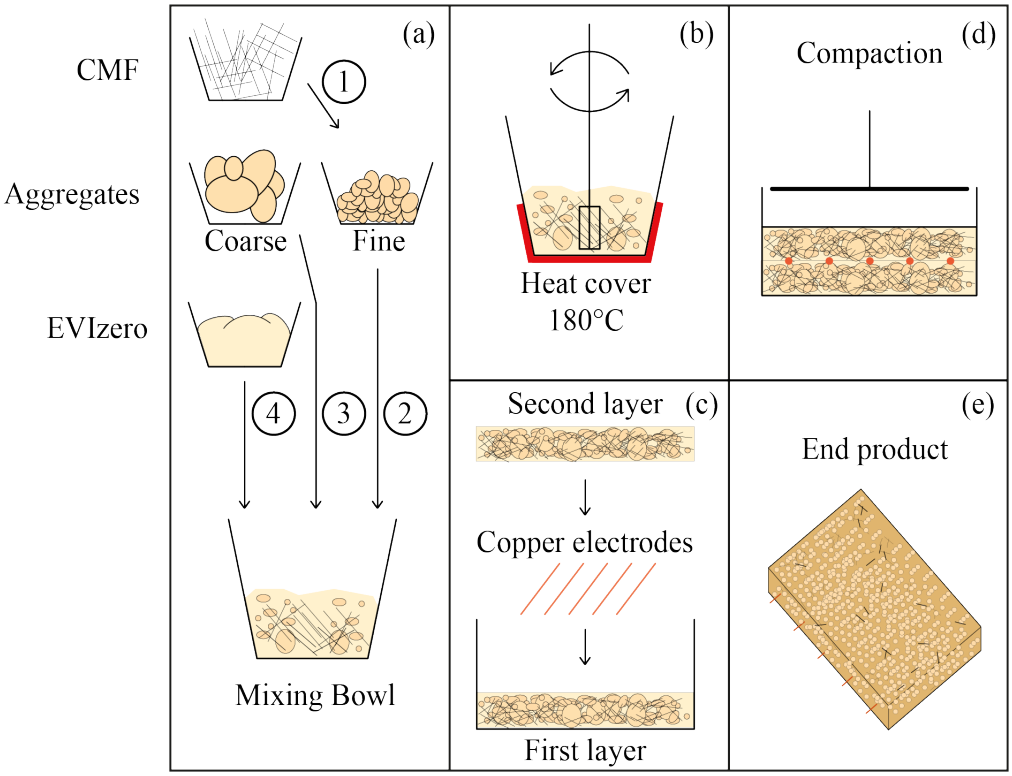

Figure 1. Smart pavement fabrication steps: (**a**) Mixing of dry materials with the melted EVIzero; (**b**) mechanical mixing under 180 °C; (**c**) casting of sample; (**d**) compaction of sample; and (**e**) smart slab constructed from half of the compaction sample.

Table 2. Mix design of the composite for one plate sample.

Components	**Aggregates (Ancona Bianco)**				**EVIzero**	**CMF**
	Fine		**Coarse**			
size	0.5–1 mm	1–2 mm	2–4 mm	4–8 mm	640	13
weight (g)	1500	2500	3000	3000		

All the aggregates are initially heated under 180 °C for 3 h, and EVIzero, molds, metal mixing bowl and other necessary metal equipment are put in the oven for one hour under the same temperature. The hot mixture is produced by mixing CMF with the fine aggregates inside the metal mixing bowl, after which the coarse aggregates are added and mixed followed by the melted EVIzero (Figure 1a). Subsequently, materials are mixed using an electric mixer inside the metal bowl seated inside the electric heater cover set at 180 °C to keep the materials under mixing temperature. The mixing continued until homogeneity is achieved (Figure 1b). Half of the mixture is cast into a rectangular mold of base dimensions 40 cm × 30 cm to form the bottom layer. Five 1 mm diameter copper electrodes of 40 cm length are placed into the cast mix at a mutual distance of 6 cm. Then, the rest of the mixture is casted (Figure 1c). The sample is compacted using an Advantest Controls Model 77-PV41A02 Slab Compactor under 160 °C until a 3.5 cm thickness is reached, which corresponds to a 2.6 g/cm^3 density (Figure 1d). After cooling down, the sample is cut in half along its long side, and the electrode tips are made accessible for wire connections by removing the material around them. At the end, two samples are produced, each measuring 30 cm × 20 cm × 3.5 cm (Figure 1e).

Small fragments of the material are taken from the final product and inspected under an optical microscope to analyze the quality of dispersion. Figure 2 shows that CMF particles do not form agglomerations and are homogeneously dispersed inside the EVIzero binder matrix.

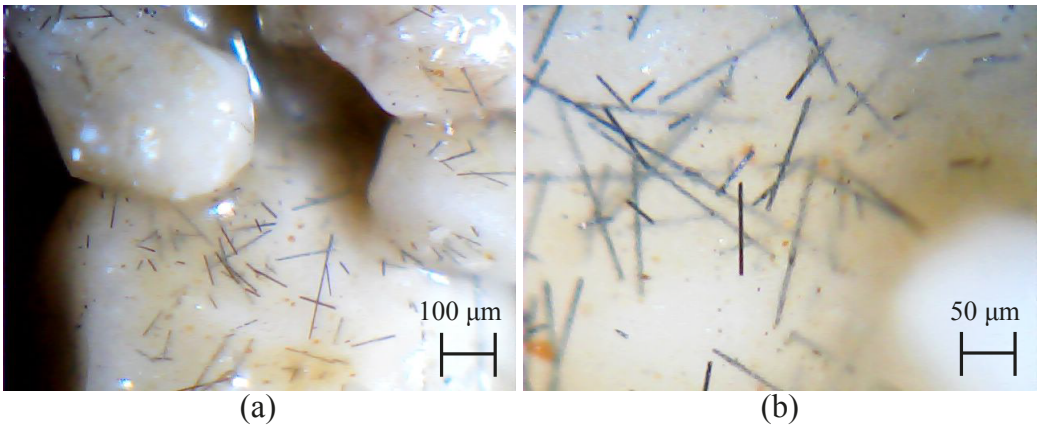

Figure 2. The dispersion of CMF inside EVIzero matrix: (**a**) CMF together with aggregates inside EVIzero; (**b**) zoomed view.

2.2. Electrical Models

The use of 5 lines of electrodes enables the configuration of the electrical setup to conduct load localization (the LL case), load magnitude sensing (the LM case), and waveform sensing (the WF case) [46]. Figure 3 schematizes the equivalent circuit configurations under these three cases, where the samples are electrically represented as resistors connected in series.

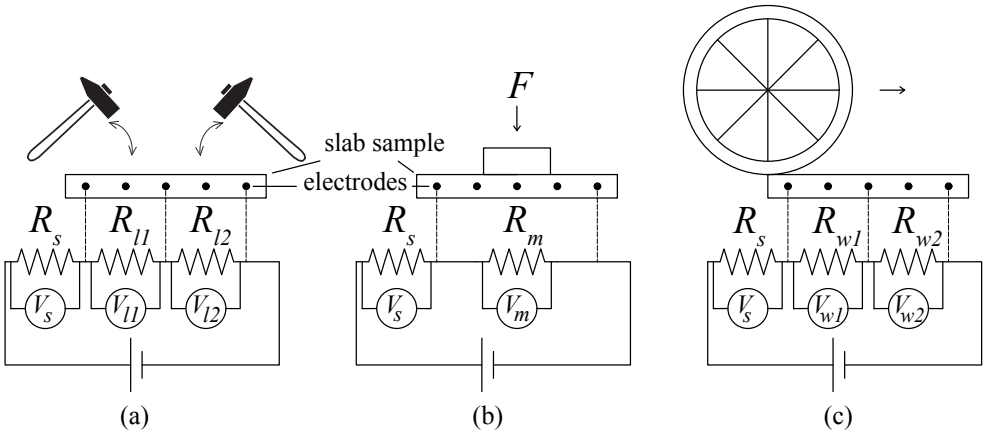

Figure 3. The equivalent circuit models for: (**a**) the LL case; (**b**) the LM case; and (**c**) the WF case.

The LL case (Figure 3a) has a shunt resistor $R_s = 1$ MΩ connected in series with the pavement sample. The circuit is powered using a DC analog input (V_i) and three voltage time history values are recorded, $V_s(t)$, $V_{l1}(t)$, and $V_{l2}(t)$, where V_s is the voltage drop through the shunt resistor, V_{l1} is the voltage drop through the first half of the sample, and V_{l2} is the voltage drop through second half of the sample. For LM and WF cases, the recorded voltage time histories are $V_m(t)$, $V_{w1}(t)$ and $V_{w2}(t)$, where V_m is the voltage drop through the whole sample and V_{w1} and V_{w2} are, respectively, identical to V_{l1} and V_{l2}. Using Ohm's law and taking R_s constant:

$$R_{l1}(t) = R_s \cdot \frac{V_{l1}(t)}{V_s(t)}$$
$$R_{l2}(t) = R_s \cdot \frac{V_{l2}(t)}{V_s(t)} \quad (1)$$

Expanding the same approach to the LM case (Figure 3b), Ohm's law yields:

$$R_m(t) = R_s \cdot \frac{V_m(t)}{V_s(t)} \quad (2)$$

The variation in the acquired voltage time histories, $V_{l1}(t)$, $V_{l2}(t)$, $V_m(t)$, $V_s(t)$ are explained by variations of resistances R_{l1}, R_{l2} and R_m due to the loads' variations caused by pressure loads placed on the sample surface. Under the WF case, data are spatio-temporally compared to assess the moving load:

$$V_r(t) = \frac{V_{w1}(t) - V_{w2}(t)}{\sum V} \quad (3)$$

where V_{w1} and V_{w2} are the voltage drops through first and second halves of the sample, respectively, with the sum normalized using $\sum V$ to obtain a reading independent from the input voltage. From Equation (3), the reading voltage time history, $V_r(t)$, is a waveform that depends on location and magnitude of the load [46]. In other words, the WF case can be viewed as the combination of the LL and LM cases.

2.3. Experimental Method

A National Instruments NI-PXI-1092 chassis capable of sourcing analog outputs and reading analog inputs is used to conduct the experiments. Samples are charged using the analog source unit PXIe-4138, capable of outputting 60 V DC of voltage and 3 A of current. The analog inputs are read through the 24-bit analog-to-digital converter PXIe-4302. The programming of the DAQ is conducted in the LABVIEW environment.

Three loading scenarios are investigated (Figure 4). In the first scenario, an impact hammer is used to hit the sample at various locations for evaluating load localization (the LL case). In the second scenario, a hand-operated hydraulic press of 20-ton maximum load capacity is used to apply loads of different magnitudes for evaluating the load magnitude sensing (the LM case), with the load of the hydraulic press read through a LAUMAS load cell. In the third scenario, a bicycle is passed over the sample placed onto the ground with or without a rider at two different speeds for evaluating waveform sensing (the WF case). A 5 V DC analog input is selected for the LL and LM cases where the experiment is conducted inside a laboratory under a controlled environment. Under the WF case, the DC voltage input is raised to 20 V in order to reduce the effect of ambient noise.

(a) (b) (c)

Figure 4. Loading methods: (**a**) the LL case—impact hammer; (**b**) the LM case—hydraulic press; and (**c**) the WF case—rolling bicycle.

3. Experimental Results

3.1. Electrical Stability

The first step in the experimental investigation is to study the electrical stability of the composite to determine if the materials suffer from the polarization effect commonly found in other types of materials such as cement-based ones. Polarization manifests itself as a temporal increase in the resistance in unloading conditions. While it is possible to reduce or even eliminate polarization for cement-based materials using dedicated measurement methods such as the biphasic input voltage measurement method presented in [37], polarization is only a concern in the measurement of static loads, because it can be assumed that the electrical steady state is already reached prior taking dynamic measurements. Nevertheless, the phenomenon needs to be assessed a priori, because it may occur over very long periods of time, necessitating long times of charging prior to take measurements. Figure 5 plots the time history of the relative change in voltage read on the unloaded composite sample over a period of 3 min. From the signal, it can be observed that the polarization period is approximately 5 s during the initial charging of the sample. Once the polarization is completed, the sample provides a stable signal under DC voltage, remaining within the range of $0.0003 \pm 0.0002 \Delta V / V_0$, equivalent to a negligible variation.

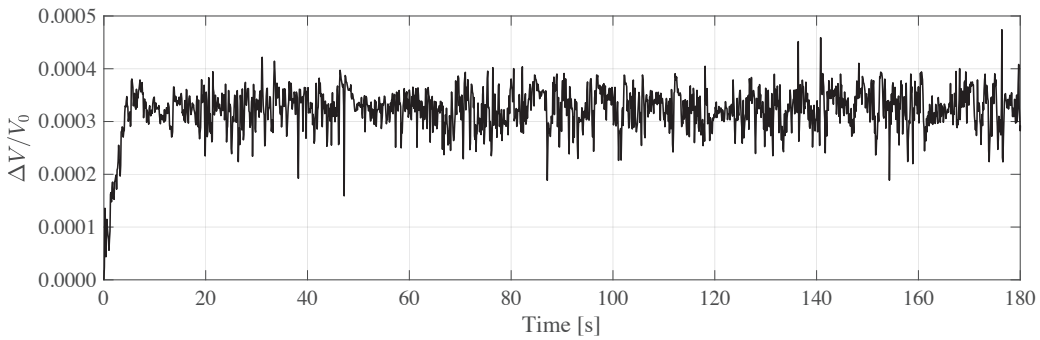

Figure 5. Variation of voltage during the electrical tests showing rapid reach of electrical steady state with no drift.

The proposed pavement carbon-doped composite has a short initial polarization time compared to the foreseen measurement periods, therefore regular DC input can be utilized for sensing, supporting high resolution and rapid load detection. To realize the sensing circuit, 5 V and 20 V DC voltage inputs are selected. The shunt resistor of 1 MΩ is selected to avoid the loss of meaningful data in the noise, which likely occurs if the difference in resistance between shunt resistor and the tested sample is significant.

3.2. Load Localization and Load Measurement

The second step of the study is to study the capability of the smart pavement to detect (the LL case) and localize (the LM case) a load. the LL case is the configuration proposed for load localization on the sample surface. For the LL case, the sample is divided into two sensing regions, and the hammer impact is applied two consecutive times on the left (Figure 6a), then three consecutive times on the right, and followed by two consecutive times on the left, in order to validate the output consistency. The sequence is repeated twice. The related voltage pulses generated during the experiments are plotted in Figure 6b,c. Results exhibit magnitudes and directions of voltage pulse that strongly correlate with the impact location: the region of impact generates a positive pulse, while the other region generates a negative pulse. Results also appear repeatable in terms of pulse intensity and direction, although the approximate force used during the impacts makes it difficult to quantify.

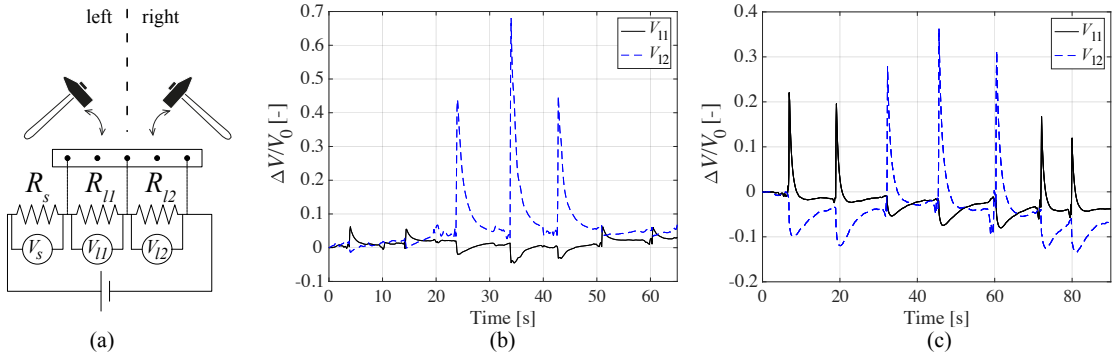

Figure 6. The sketch of the experiment (**a**) and the voltage pulses generated during two hammer-impact test sequences (**b**,**c**).

Figure 7 presents results from the LM case, showing the voltage pulses generated by rapid loading–unloading of increasing load magnitudes using a hand-controlled hydraulic press at the middle of the sample over a 10 cm × 10 cm square steel plate electrically insulated. The voltage of the sensing circuit is set to 5 V. The results clearly show that the voltage pulse amplitude is strongly dependent on the applied load magnitude and the response is linear. Note that differences of voltage between the LM case and the LL and WF cases are attributable to the differences in sample section sizes being measured.

Results show that composite sample is capable of localizing and quantifying the applied load. The next experimental phase is to subject the sample to a moving load (the WF case).

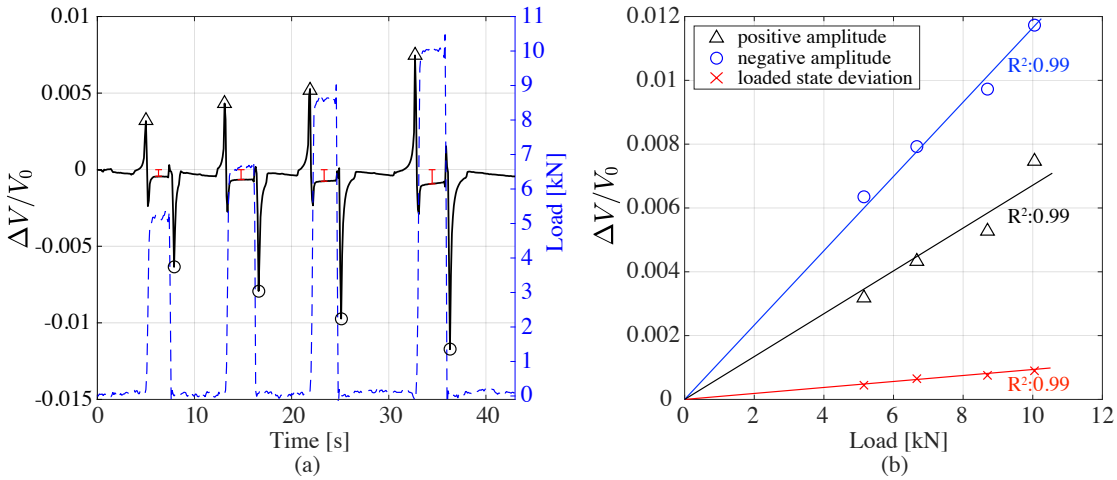

Figure 7. The results of the rapid loading–unloading tests done on the pavement sample (the LM case): (**a**) the generated voltage pulses along with loading–unloading pattern, where the red lines represent the deviation from 0 during the loaded period of the sample; (**b**) readings of positive and negative amplitude peaks and deviation from unloaded state along with the linear fits and R^2 values.

3.3. Weigh-In-Motion Sensing

The WF case is evaluated through four different load events generated by the passage of a bicycle: (1) fast-unloaded; (2) slow-unloaded; (3) fast-loaded; and (4) slow-loaded, where fast/slow indicates the speed of the bicycle and loaded/unloaded indicates the presence of a rider. For the unloaded events, the bicycle is rolled over the sample using an operator standing next to the sample. For the loaded events, the rider is on the bicycle and adds a gross weight of approximately 58 kg. All the passages are performed within a single data collection period. The recorded response is plotted in Figure 8.

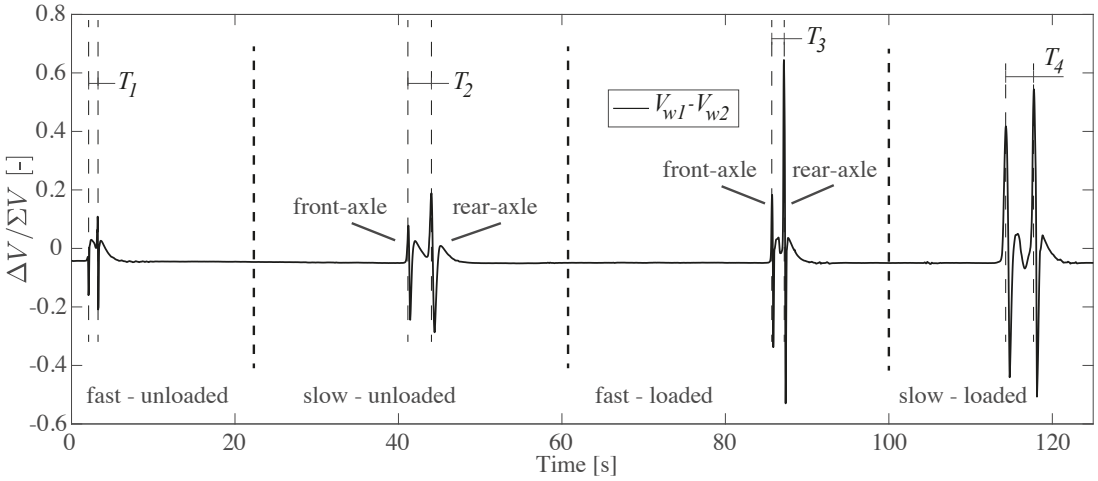

Figure 8. Time series of voltage pulses obtained from the pavement sample during the bicycle pass tests, showing the ratio ΔV to the total read voltage (ΣV) and the time period between front and rear axle occurrences T.

Several observations can be made from the results: (1) scaled and repetitive behaviour generated by the pavement sample is similar to that shown in Figure 7; (2) pulse amplitudes for the unloaded and loaded responses are consistent; (3) pulse amplitudes differ consistently with the presence of bicycle driver; (4) all waveforms are similar in shape but temporally stretched with the varying speed; (5) signal amplitudes are large, especially during the loaded passages of the bicycle, with the spikes explained by the instant body deformations of the pavement caused by not perfect grip on ground; (6) general recursive voltage pulse responses are generated from bicycle loads; (7) voltage pulses reflect the load magnitude and speed, with the axle occurrences being detectable; (8) peak-to-peak temporal distances corresponding to the slow passages (T_2 and T_4) are significantly longer than those corresponding to fast passages (T_1 and T_3); and (9) the voltage difference time history patterns are found repetitive and consistent, hence suitable for the characterization of the methodologies [47]. The characterization values obtained from the tests are presented in Table 3. Accordingly, voltage pulses increase significantly with the presence of rider weight, the calculated increase ratios are observed to be suitable for distinction between load states of bicycle even for the relatively small loads compared with traffic loads.

Table 3. Characteristics of loads and signal response from the bicycle passing tests. The values obtained from unloaded and loaded cases are listed together with the loaded/unloaded ratio.

Weight Case	**Unloaded**		**Loaded**		**Ratio**	
Speed Case	**Fast**	**Slow**	**Fast**	**Slow**	**Fast**	**Slow**
axle occurrence time difference (s)	1.19	3.00	1.47	3.35	-	-
front axle pos. pulse magnitude ($V/\Sigma V$)	0.013	0.123	0.230	0.461	-	3.75
front axle neg. pulse magnitude ($V/\Sigma V$)	0.120	0.204	0.288	0.398	2.40	1.95
rear axle pos. pulse magnitude ($V/\Sigma V$)	0.170	0.246	0.780	0.593	4.59	2.41
rear axle neg. pulse magnitude ($V/\Sigma V$)	0.192	0.244	0.534	0.464	2.78	1.90
weight of the bicycle (kg)	20		78		3.90	

To further evaluate the sensing capabilities of the composite pavement unit more, the acquired signals V_{w1} and V_{w2} are plotted in Figure 9 for the loaded cases. It is observed that there is a time shift between the occurrences of peaks indicated by τ_i. This time shift is related to the speed of the bicycle.

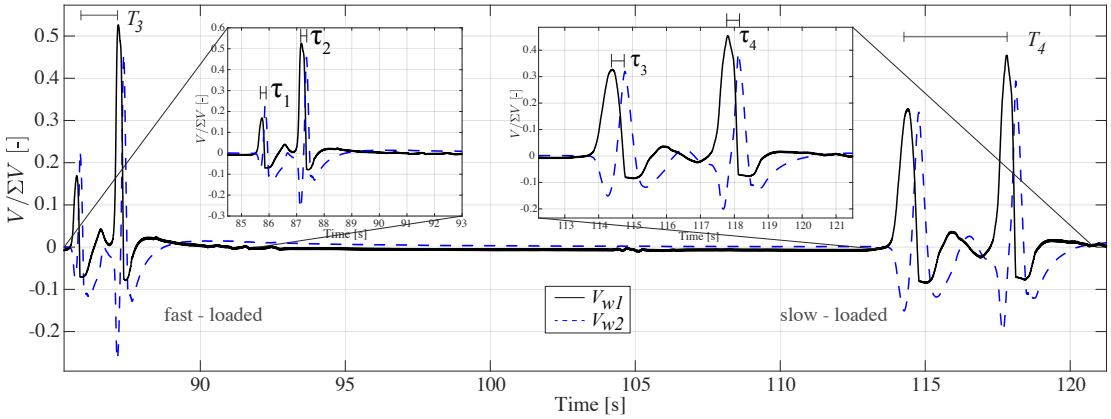

Figure 9. Relative time histories of V_{w1} and V_{w2} showing time shifts between peaks of the signals.

Data shown plotted in Figure 9 can be used to calculate the axle spacing (l_{ax}) of the bicycle. The distance between the midpoints of each half is taken as the reference length for spatial measurement, that is 12 cm (δ). The ratio of time shifts T from Figure 8 and average τ ($\bar{\tau}$) from Figure 9 is defined as the geometry constant (γ). The average τ ($\bar{\tau}$) is calculated by averaging the two values of τ coming from both signal peaks of a bicycle passing. Equation (4) is employed for calculations

$$l_{ax} = \delta \cdot \frac{T}{\bar{\tau}} = \delta \cdot \gamma \tag{4}$$

Results are listed in Table 4. Accordingly, the real distance between axles is measured as 1.08 m. The distances calculated using measurements are found to be 1.10 m and 1.15 m for the fast and slow passings, respectively, yielding an average error of 5%.

Table 4. Bicycle geometry characterization according to the loaded passings. T denotes the time period between axle occurrences on the pavement and τ_i denotes the time shift between recordings coming from different segments of pavement.

Passing Type	Fast	Slow
axle occurrence time diff. (s)	T_3 = 1.47	T_4 = 3.35
axle moving time diff. (s)	τ_1 = 0.18 τ_2 = 0.14	τ_3= 0.4 τ_4= 0.3
average, $\bar{\tau}$ (s)	0.16	0.35
geometry const. (γ)	9.19	9.57
axle spacing, l_{ax} (m)	1.10	1.15
real spacing (m)	1.08	1.08
error	2%	7%

4. Discussion

In this study, a new smart composite for weigh-in-motion in road pavements is proposed, consisting of a commercial eco-friendly synthetic binder, named EVIzero, doped with carbon microfibers. The new material is tested considering a plate sample with dimensions of 30 cm × 20 cm × 3.5 cm. Test results show that: (i) the sample is able to localize the impact loads on its surface, (ii) the sample generates signals scaled to the applied load magnitude, (iii) the sample can differentiate between fast/slow and loaded/unloaded passing loads. Expanding the discussion, the proposed composite has significant advances over traditional self-sensing cementitious materials. Firstly, the production of the proposed sensing material requires only mechanical mixing. In that way, the material can be manufactured and applied directly on the field like a regular pavement. Secondly, fast polarization and rapid transition to steady state is observed under the DC voltage input, resulting in a material suitable for dynamic load sensing without being affected by the sampling rate of the biphasic voltage input. Aside from being beneficial

for high resolution sensing, the usage of DC voltage allows to employ less complex data acquisition systems for the designed pavement sensors: this occurrence highly increases the field applicability by reducing installation challenges and costs. Thirdly, the response to applied load is rapid and without lags, indicating that traffic loads are recognizable by the sensing system, when sufficient resolution is provided.

During the experiments, the responses acquired for different sensing in the LL, LM and WF cases are highly repeatable. The signal magnitude differs greatly between the LL, WF and LM cases, likely due to the following reasons: (i) the measurement types of sample body are different; and (ii) the LM case is conducted inside a press machine in fixed support conditions, while in the WF case the sample is vulnerable to the body deformations. Such body deformations are critical and may have significant influence on the characterization algorithms when the design is not adequately carried out. It is concluded that more reliable outcomes are attainable from this composite when embedded within the road and supported by rigid ground and optimal setup. This investigation is foreseen to be the part of the next study investigating the field performance of the proposed WIM technology.

5. Conclusions

This paper presented the results of an investigation on self-sensing properties of an innovative carbon composites for WIM applications. A multi-functional piezo-resistive load sensing pavement material has been proposed by mixing a synthetic binder material with aggregates and carbon microfibers. A smart pavement plate sample was fabricated and subjected to an experimental campaign that included hammer impacts, load controlled tests and bicycle passes. The obtained signal responses were found consistent and scaled to the load magnitude. The response was fast and the material did not suffer significantly from polarization under the DC voltage input.

Thus, experiments revealed that a traffic load sensor made of the proposed pavement composite and setup are promising candidates in terms of cost efficiency, easiness of implementation, durability and precision. With the tailored electrode's distribution inside the pavement, the composite can sense the speed and thus serve to reduce the total number of sensors used for a WIM characterization of vehicles and simplify the monitoring of infrastructure. In this context, results from the dynamic test indicated that one sensor was enough to calculate axle separation distance. The next steps in the research will include the optimization of the composite for both the mechanical and electrical properties, as well as field validation on roadway infrastructure.

Author Contributions: Following contributions are made by authors; conceptualization, F.U. and S.L.; methodology, H.B.B. and A.D.; software, H.B.B.; validation, A.D., S.L. and F.U.; resources, F.U.; writing—original draft preparation, H.B.B.; writing—review and editing, A.D., S.L. and F.U.; visualization, H.B.B. and A.D.; supervision, S.L. and F.U. All authors have read and agreed to the published version of the manuscript.

Funding: This research has received funding from the European Union's Horizon 2020 research and innovation programme under Grant Agreement N. 765057-SAFERUP! Project.

Institutional Review Board Statement: Not applicable.

Informed Consent Statement: Not applicable.

Data Availability Statement: The data that support the findings of this study are available from the corresponding author, A.D., upon reasonable request.

Acknowledgments: The authors would like to acknowledge the support of Corecom s.r.l, with a special thanks to Maurizio Favaro, for providing testing material, and for the consultation on material fabrication.

Conflicts of Interest: The authors declare no conflict of interest.

References

1. Frangopol, D.M.; Strauss, A.; Kim, S. Bridge reliability assessment based on monitoring. *J. Bridge Eng.* **2008**, *13*, 258–270. [CrossRef]
2. Guo, T.; Frangopol, D.M.; Chen, Y. Fatigue reliability assessment of steel bridge details integrating weigh-in-motion data and probabilistic finite element analysis. *Comput. Struct.* **2012**, *112*, 245–257. [CrossRef]
3. Marsh, G.; Wignall, C.; Thies, P.R.; Barltrop, N.; Incecik, A.; Venugopal, V.; Johanning, L. Review and application of Rainflow residue processing techniques for accurate fatigue damage estimation. *Int. J. Fatigue* **2016**, *82*, 757–765. [CrossRef]
4. Hou, R.; Dedhia, Y.A.; Jeong, S.; Law, K.; Ettouney, M.; Lynch, J.P. Fusion of weigh-in-motion system and bridge monitoring data for bridge load rating. In Proceedings of the 9th International Conference on Structural Health Monitoring of Intelligent Infrastructure, St. Louis, MO, USA, 4–7 August 2019.
5. Croce, P. Impact of road traffic tendency in europe on fatigue assessment of bridges. *Appl. Sci.* **2020**, *10*, 1389. [CrossRef]
6. Deng, L.; Wang, W.; Yu, Y. State-of-the-art review on the causes and mechanisms of bridge collapse. *J. Perform. Constr. Facil.* **2016**, *30*, 04015005. [CrossRef]
7. Jacob, B.; Feypell-de La Beaumelle, V. Improving truck safety: Potential of weigh-in-motion technology. *IATSS Res.* **2010**, *34*, 9–15. [CrossRef]
8. Wang, J.; Wu, M. An overview of research on weigh-in-motion system. In Proceedings of the Fifth World Congress on Intelligent Control and Automation (IEEE Cat. No. 04EX788), Hangzhou, China, 15–19 June 2004; Volume 6, pp. 5241–5244.
9. Yu, Y.; Cai, C.; Deng, L. State-of-the-art review on bridge weigh-in-motion technology. *Adv. Struct. Eng.* **2016**, *19*, 1514–1530. [CrossRef]
10. Zhu, B.; Frangopol, D.M. Risk-based approach for optimum maintenance of bridges under traffic and earthquake loads. *J. Struct. Eng.* **2013**, *139*, 422–434. [CrossRef]
11. Burnos, P.; Gajda, J. Thermal property analysis of axle load sensors for weighing vehicles in weigh-in-motion system. *Sensors* **2016**, *16*, 2143. [CrossRef]
12. Xue, W.; Wang, D.; Wang, L. A review and perspective about pavement monitoring. *Int. J. Pavement Res. Technol* **2012**, *5*, 295–302.
13. Sekuła, K.; Kołakowski, P. Piezo-based weigh-in-motion system for the railway transport. *Struct. Control Health Monit.* **2012**, *19*, 199–215. [CrossRef]
14. Xiong, H.; Zhang, Y. Feasibility study for using piezoelectric-based weigh-in-motion (WIM) system on public roadway. *Appl. Sci.* **2019**, *9*, 3098. [CrossRef]
15. Al-Tarawneh, M.; Huang, Y. In-pavement fiber Bragg grating sensors for high-speed weigh-in-motion measurements. In Proceedings of the Sensors and Smart Structures Technologies for Civil, Mechanical, and Aerospace Systems 2017, Portland, OR, USA, 26–29 March 2017; Volume 10168, p. 101681Y.
16. Zhao, H.; Uddin, N.; Shao, X.; Zhu, P.; Tan, C. Field-calibrated influence lines for improved axle weight identification with a bridge weigh-in-motion system. *Struct. Infrastruct. Eng.* **2015**, *11*, 721–743. [CrossRef]
17. Bao, T.; Babanajad, S.K.; Taylor, T.; Ansari, F. Generalized method and monitoring technique for shear-strain-based bridge weigh-in-motion. *J. Bridge Eng.* **2016**, *21*, 04015029. [CrossRef]
18. Lydon, M.; Robinson, D.; Taylor, S.; Amato, G.; Brien, E.; Uddin, N. Improved axle detection for bridge weigh-in-motion systems using fiber optic sensors. *J. Civ. Struct. Health Monit.* **2017**, *7*, 325–332. [CrossRef]
19. Chen, S.Z.; Wu, G.; Feng, D.C.; Zhang, L. Development of a bridge weigh-in-motion system based on long-gauge fiber Bragg grating sensors. *J. Bridge Eng.* **2018**, *23*, 04018063. [CrossRef]
20. Pimentel, R.; Ribeiro, D.; Matos, L.; Mosleh, A.; Calçada, R. *Bridge Weigh-In-Motion System for the Identification of Train Loads Using Fiber-Optic Technology*; Elsevier: Amsterdam, The Netherlands, 2021; Volume 30, pp. 1056–1070.
21. Sekiya, H.; Kubota, K.; Miki, C. Simplified portable bridge weigh-in-motion system using accelerometers. *J. Bridge Eng.* **2018**, *23*, 04017124. [CrossRef]
22. OBrien, E.; Khan, M.A.; McCrum, D.P.; Žnidarič, A. Using statistical analysis of an acceleration-based bridge weigh-in-motion system for damage detection. *Appl. Sci.* **2020**, *10*, 663. [CrossRef]
23. Mustafa, S.; Sekiya, H.; Hirano, S.; Miki, C. Iterative linear optimization method for bridge weigh-in-motion systems using accelerometers. *Struct. Infrastruct. Eng.* **2020**. [CrossRef]
24. Ojio, T.; Carey, C.; OBrien, E.J.; Doherty, C.; Taylor, S.E. Contactless bridge weigh-in-motion. *J. Bridge Eng.* **2016**, *21*, 04016032. [CrossRef]
25. Bajwa, R.; Coleri, E.; Rajagopal, R.; Varaiya, P.; Flores, C. Development of a cost-effective wireless vibration weigh-in-motion system to estimate axle weights of trucks. *Comput.-Aided Civ. Infrastruct. Eng.* **2017**, *32*, 443–457. [CrossRef]
26. Dontu, A.; Barsanescu, P.; Andrusca, L.; Danila, N. Weigh-in-motion sensors and traffic monitoring systems-Sate of the art and development trends. In Proceedings of the IOP Conference Series: Materials Science and Engineering, Chennai, India, 16–17 September 2020; Volume 997, p. 012113.
27. Han, B.; Zhang, K.; Burnham, T.; Kwon, E.; Yu, X. Integration and road tests of a self-sensing CNT concrete pavement system for traffic detection. *Smart Mater. Struct.* **2012**, *22*, 015020. [CrossRef]
28. Downey, A.; D'Alessandro, A.; Ubertini, F.; Laflamme, S. Automated crack detection in conductive smart-concrete structures using a resistor mesh model. *Meas. Sci. Technol.* **2018**, *29*, 035107. [CrossRef]

29. Tian, Z.; Li, Y.; Zheng, J.; Wang, S. A state-of-the-art on self-sensing concrete: Materials, fabrication and properties. *Compos. Part B Eng.* **2019**, *177*, 107437. [CrossRef]
30. Das, A.K.; Mishra, D.K.; Yu, J.; Leung, C.K. Smart self-healing and self-sensing cementitious composites—recent developments, challenges, and prospects. *Adv. Civ. Eng. Mater.* **2019**, *8*, 554–578. [CrossRef]
31. Laflamme, S.; Ubertini, F. Back-to-basics: Self-sensing materials for nondestructive evaluation. *Mater. Eval.* **2020**, *78*, 526–536.
32. Monteiro, A.; Costa, P.; Oeser, M.; Cachim, P. Dynamic sensing properties of a multifunctional cement composite with carbon black for traffic monitoring. *Smart Mater. Struct.* **2020**, *29*, 025023. [CrossRef]
33. del Moral, B.; Baeza, F.J.; Navarro, R.; Galao, O.; Zornoza, E.; Vera, J.; Farcas, C.; Garcés, P. Temperature and humidity influence on the strain sensing performance of hybrid carbon nanotubes and graphite cement composites. *Constr. Build. Mater.* **2021**, *284*, 122786. [CrossRef]
34. Gawel, K.; Szewczyk, D.; Cerasi, P.R. Self-Sensing Well Cement. *Materials* **2021**, *14*, 1235. [CrossRef]
35. Xu, J.; Yin, T.; Wang, Y.; Liu, L. Anisotropic electrical and piezoresistive sensing properties of cement-based sensors with aligned carbon fibers. *Cem. Concr. Compos.* **2021**, *116*, 103873. [CrossRef]
36. Dalla, P.T.; Tragazikis, I.K.; Trakakis, G.; Galiotis, C.; Dassios, K.G.; Matikas, T.E. Multifunctional Cement Mortars Enhanced with Graphene Nanoplatelets and Carbon Nanotubes. *Sensors* **2021**, *21*, 933. [CrossRef]
37. Downey, A.; D'Alessandro, A.; Ubertini, F.; Laflamme, S.; Geiger, R. Biphasic DC measurement approach for enhanced measurement stability and multi-channel sampling of self-sensing multi-functional structural materials doped with carbon-based additives. *Smart Mater. Struct.* **2017**, *26*, 065008. [CrossRef]
38. Monti, M.; Natali, M.; Petrucci, R.; Kenny, J.M.; Torre, L. Carbon nanofibers for strain and impact damage sensing in glass fiber reinforced composites based on an unsaturated polyester resin. *Polym. Compos.* **2011**, *32*, 766–775. [CrossRef]
39. Monti, M.; Armentano, I.; Faiella, G.; Antonucci, V.; Kenny, J.M.; Torre, L.; Giordano, M. Toward the microstructure–properties relationship in MWCNT/epoxy composites: Percolation behavior and dielectric spectroscopy. *Compos. Sci. Technol.* **2014**, *96*, 38–46. [CrossRef]
40. D'Alessandro, A.; Coffetti, D.; Crotti, E.; Coppola, L.; Meoni, A.; Ubertini, F. Self-Sensing Properties of Green Alkali-Activated Binders with Carbon-Based Nanoinclusions. *Sustainability* **2020**, *12*, 9916. [CrossRef]
41. Liu, X.; Wu, S.; Li, N.; Gao, B. Self-monitoring application of asphalt concrete containing graphite and carbon fibers. *J. Wuhan Univ. Technol.-Mater. Sci. Ed.* **2008**, *23*, 268–271. [CrossRef]
42. Liu, X.; Wu, S. Study on the graphite and carbon fiber modified asphalt concrete. *Constr. Build. Mater.* **2011**, *25*, 1807–1811. [CrossRef]
43. Liu, X.; Nie, Z.; Wu, S.; Wang, C. Self-monitoring application of conductive asphalt concrete under indirect tensile deformation. *Case Stud. Constr. Mater.* **2015**, *3*, 70–77. [CrossRef]
44. Corecom. EVIzero Technical Data Sheet. Available online: https://www.evizero.com/download/technical-data-sheet-evizero.pdf (accessed on 25 February 2021).
45. Carbon, S. Sigrafil Short Carbon Fibers. Available online: https://www.sglcarbon.com/en/markets-solutions/material/sigrafil-short-carbon-fibers (accessed on 25 February 2021).
46. Birgin, H.B.; Laflamme, S.; D'Alessandro, A.; Garcia-Macias, E.; Ubertini, F. A Weigh-in-Motion Characterization Algorithm for Smart Pavements Based on Conductive Cementitious Materials. *Sensors* **2020**, *20*, 659. [CrossRef]
47. Bosso, M.; Vasconcelos, K.L.; Ho, L.L.; Bernucci, L.L. Use of regression trees to predict overweight trucks from historical weigh-in-motion data. *J. Traffic Transp. Eng. (Engl. Ed.)* **2020**, *7*, 843–859. [CrossRef]